J Neuropathol Exp Neurol

Vol. 74, No. 7
July 2015
pp. 688–703

ORIGINAL ARTICLE

OPEN

Neuropathologic Characterization of Pontocerebellar Hypoplasia Type 6 Associated With Cardiomyopathy and Hydrops Fetalis and Severe Multisystem Respiratory Chain Deficiency due to Novel *RARS2* Mutations

Nichola Z. Lax, PhD, Charlotte L. Alston, BSc(Hons), Katherine Schon, MA, MRCP, Soo-Mi Park, PhD, FRCP, Deepa Krishnakumar, MRCPH, Langping He, PhD, Gavin Falkous, MPhil, Amanda Ogilvy-Stuart, DM, FRCP, Christoph Lees, MD, MRCOG, Rosalind H. King, PhD, Iain P. Hargreaves, PhD, Garry K. Brown, PhD, Robert McFarland, PhD, MRCPCH, Andrew F. Dean, PhD, and Robert W. Taylor, PhD, FRCPath

Abstract

Autosomal recessive mutations in the *RARS2* gene encoding the mitochondrial arginyl-transfer RNA synthetase cause infantile-onset myoencephalopathy pontocerebellar hypoplasia type 6 (PCH6). We describe 2 sisters with novel compound heterozygous *RARS2* mutations who presented perinatally with neurologic features typical of PCH6 but with additional features including cardiomyopathy, hydrops, and pulmonary hypoplasia and who died at 1 day and 14 days of age. Magnetic resonance imaging findings included marked cerebellar hypoplasia, gyral immaturity, punctate lesions in cerebral white matter, and unfused deep cerebral grey matter. Enzyme histochemistry of postmortem tissues revealed a near-global cytochrome *c* oxidase-deficiency; assessment of respiratory chain enzyme activities confirmed severe deficiencies involving complexes I, III, and IV. Molecular genetic studies revealed 2 *RARS2* gene mutations: a c.1A>G, p.? variant predicted to abolish the initiator methionine, and a deep intronic c.613-3927C>T variant causing skipping of exons 6–8 in the mature *RARS2* transcript. Neuropathologic investigation included low brain weights, small brainstem and cerebellum, deep cerebral white matter pathology, pontine nucleus neuron loss (in 1 sibling), and peripheral nerve pathology. Mitochondrial respiratory chain immunohistochemistry in brain tissues confirmed an absence of complexes I and IV immunoreactivity with sparing of mitochondrial numbers. These cases expand the clinical spectrum of *RARS2* mutations, including antenatal features and widespread mitochondrial respiratory chain deficiencies in postmortem brain tissues.

Key Words: Mitochondrial disease, Pontocerebellar hypoplasia type 6, *RARS2*, Respiratory chain deficiency.

INTRODUCTION

Mitochondrial respiratory chain diseases represent a clinically and genetically diverse collection of isolated or multiorgan disorders with an incidence estimated at 1 in 5000 births (1). Mutations in either mitochondrial or nuclear DNA can lead to defective protein synthesis resulting in impaired assembly and function of the oxidative phosphorylation system and reduced adenine triphosphate biosynthesis. This can

From the Wellcome Trust Centre for Mitochondrial Research, Institute of Neuroscience, The Medical School, Newcastle University, Newcastle upon Tyne, UK (NZL, CLA, LH, GF, RM, RWT); East Anglian Medical Genetics Service, Cambridge University Hospital NHS foundations Trust, Cambridge Biomedical Campus, Cambridge, UK (KS, SP); Department of Paediatric Neurology, Addenbrooke's Hospital, Cambridge Biomedical Campus, Cambridge UK (DK); Neonatal Unit, The Rosie Hospital, Cambridge University Hospitals NHS Foundation Trust, Cambridge, UK (AO); The Centre for Fetal Care, Queen Charlotte's and Chelsea Hospital, Du Cane Road, London, UK (CL); Department of Clinical Neurosciences, Institute of Neurology, University College London, London, UK (RHK); Neurometabolic Unit, National Hospital for Neurology and Neurosurgery, London, UK (IPH); Oxford Medical Genetics Laboratories, Oxford University Hospitals NHS Trust, Oxford, UK (GKB); and Department of Histopathology, Cambridge University Hospital NHS foundations Trust, Cambridge, UK (AFD).

Send correspondence and reprint requests to: Robert W. Taylor, PhD, FRCPath, Wellcome Trust Centre for Mitochondrial Research, Institute of Neuroscience, Newcastle University, Medical School, Framlington Place, Newcastle upon Tyne NE2 4HH United Kingdom; E-mail: robert.taylor@ncl.ac.uk

These authors contributed equally to the work: Nichola Z. Lax, PhD, Charlotte L. Alston, BSc(Hons).

Disclosure of funding: This work was supported by grants (to RWT and RM) from The Wellcome Trust Centre for Mitochondrial Research (096919Z/11/Z), the Medical Research Council (UK) Centre for Translational Muscle Disease Research (G0601943), The Lily Foundation and the UK NHS Highly Specialised Commissioners which funds the ''Rare Mitochondrial Disorders of Adults and Children'' Diagnostic Service in Newcastle upon Tyne (http://www.mitoresearch.org.uk/). CLA is the recipient of a National Institute for Health Research (NIHR) doctoral fellowship (NIHR-HCS-D12-03-04). CL is supported by the National Institute for Health Research (NIHR) Biomedical Research Centre based at Imperial College Healthcare NHS Trust and Imperial College London. The views expressed are those of the author(s) and not necessarily those of the NHS, the NIHR or the Department of Health.

Supplemental digital content is available for this article. Direct URL citations appear in the printed text and are provided in the HTML and PDF versions of this article on the journal's Web site (www.jneuropath.com).

result in a wide range of phenotypes affecting both children and adults. The increasing use of targeted exome sequencing and next-generation sequencing has led to the identification of an expanding spectrum of mutations in nuclear encoded mitochondrial proteins (2), including mitochondrial aminoacyl transfer RNA (tRNA) synthetases (mt-aaRSs) (3).

All mt-aaRSs are translated in the cytosol before being imported into the mitochondria where they play a key role in mitochondrial protein translation by catalyzing the attachment of amino acids to their cognate tRNA molecules. This is a 2-step process by which the mt-aaRS activates 1 of the 20 amino acids with adenine triphosphate to form an aminoacyl-adenylate intermediate, which then transfers the aminoacyl part to the cognate tRNA. Once a tRNA is charged with its cognate amino acid, it is delivered to the mitoribosome where the amino acid can become incorporated into the growing polypeptide chain (4).

Defects in mt-aaRSs have emerged as an important cause of perinatal or infantile onset respiratory chain diseases. These are associated with autosomal recessive inheritance and are often fatal in early life. Mutations in *RARS2* (mitochondrial arginyl-tRNA synthetase; 6q15) have been identified in children with pontocerebellar hypoplasia type 6 ([PCH6]; OMIM#611523); these were first described in a consanguineous Sephardic Jewish family in which affected children presented with intractable seizures, hypotonia, profound neurodevelopmental delay, microcephaly, and feeding difficulties (5). Neuroimaging revealed progressive cerebellar atrophy with cerebral involvement. Each affected child was homozygous for an intronic c.110+5A>G mutation leading to aberrant mRNA splicing and associated with respiratory chain defects in muscle and fibroblasts. An additional 16 patients harboring autosomal recessive *RARS2* mutations have since been reported (6–10); detailed postmortem neuropathologic reports are only available for 2 cases (11). These cases demonstrated additional features of PCH subtypes 2 and 4, including severe dystonia, optic atrophy, and thinning of the corpus callosum (9). In addition to the PCH, anterior horn cell disease was also found at autopsy, a finding typically associated with PCH1 (7).

Here we report 2 siblings with a PCH6 presentation in whom, in addition to the characteristic pontocerebellar hypoplasia and microcephaly, there was evidence of cardiomyopathy and peripheral neuropathy. We show that this fatal neurologic disease was due to novel compound heterozygous *RARS2* mutations, including the first deep intronic recessive mutation to cause fatal pediatric mitochondrial disease, and describe the neuropathologic characteristics in postmortem brain tissue from both clinically affected siblings.

MATERIALS AND METHODS

This study had relevant ethical approval from the institutional review board of Newcastle University and complied with the Declaration of Helsinki, and written informed consent was obtained.

Patients

Patient I-1

A female was born at 36 weeks to nonconsanguineous healthy, UK Caucasian British parents following a normal pregnancy and delivery. Birth weight was 2.470 kg (25th–50th centile); head circumference was 32.5 cm (50th–75th centile). On delivery, general condition was immediately and unexpectedly poor, with Apgar scores of 1 at 1 minute and 1 at 5 minutes. She was blue, floppy, and took only 1 breath. She was intubated at birth, and resuscitation was attempted for over an hour but was ultimately unsuccessful. Apart from a dermal pit on the lower back, no dysmorphic features were noted on examination.

Patient I-2

This pregnancy was closely monitored because of the previous neonatal death. Nuchal translucency was increased on ultrasound at 12 weeks (3.8 mm; 99th centile, 3.5 mm [12]). Because of concerns about fetal bradycardia, serial fetal echocardiograms were performed, which, at 20 weeks gestation, revealed mild biventricular hypertrophy in the absence of left or right outflow obstruction. From 29 weeks on the ventricular hypertrophy was more marked on the right than the left and was nonprogressive. Ultrasonography revealed transverse cerebellar diameter at 18.9 mm at 20^{+2} weeks and 19.5mm at 21^{+2} weeks on the 3rd percentile. Biparietal diameter was 43.8 and 49.6 mm at corresponding dates. Repeat ultrasound scan at 36 weeks showed polyhydramnios, right-sided pleural effusion, hyperechogenic bowel loops with bowel dilation, skin edema, and absence of fetal movements.

Labor was induced at 36^{+2} weeks, with vaginal delivery of a cyanotic, hypotonic, and bradycardic female weighing 2.340 kg (25th centile). APGAR scores were 3 at 1 minute and 4 at 5 minutes. Assisted ventilation rapidly improved both heart rate and color. She was intubated by 6 minutes of age because of absence of echocardiogram movements and absent respiratory effort. She remained ventilator dependent. Postnatal echocardiogram confirmed biventricular hypertrophy with good ventricular function and neither left nor right ventricular outflow obstruction. Neurologic examination revealed marked central and peripheral hypotonia, decreased reflexes and minimal spontaneous limb movements. No dysmorphic features were noted. Ocular and audiologic examinations were normal. On day 2, EEG suggested burst-suppression pattern. Blood and CSF lactate levels were elevated (blood persistently ~7 mmol/L with maximum 19.8 mmol/L on day 11 [reference range, 0.7–2.2 mmol/L], CSF 11.3 mmol/L on day 5 [reference range, 1.1–2.2 mmol/L]). She had low serum calcium on day 1 treated with intravenous calcium infusion and hyponatremia during the first week managed by fluid restriction. Urinary analyses showed moderate lactic aciduria, moderately increased 4-hydroxyphenylacetate, and mildly increased 4-hydroxyphenylpyruvate, consistent with liver dysfunction/immaturity. Cranial magnetic resonance imaging (MRI) was performed on day 8. After family discussion, intensive care was withdrawn on day 14, and death rapidly occurred. A full postmortem examination was conducted 1 day later with full consent.

Muscle Histology, Histochemistry, and Respiratory Chain Activity

Standard histologic and histochemical analyses of postmortem skeletal muscle and cardiac tissue were performed on

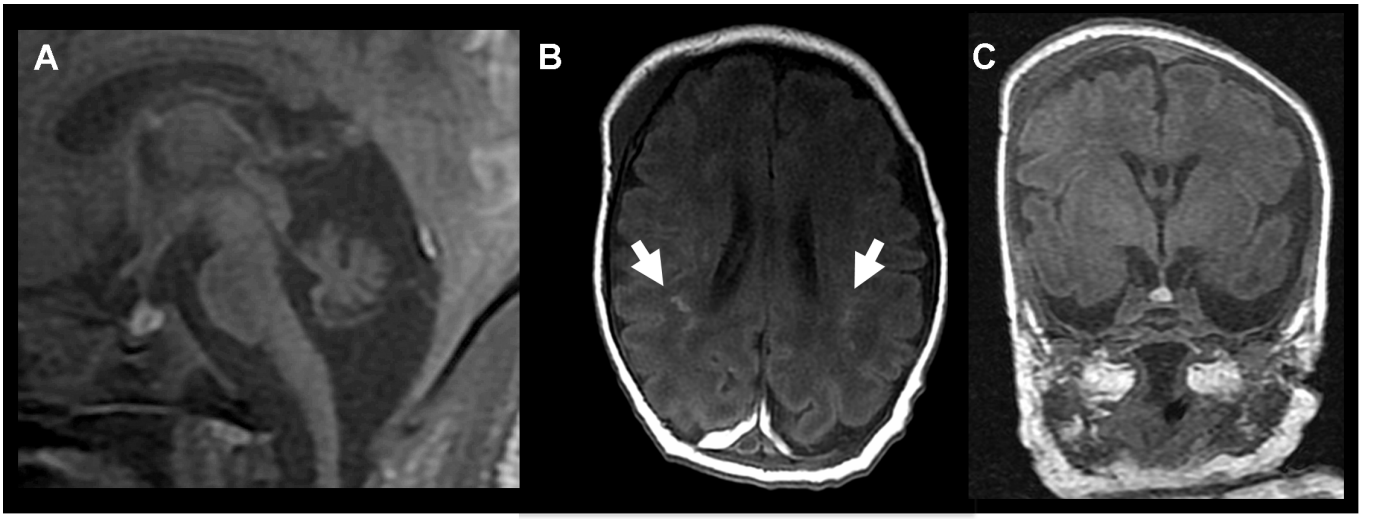

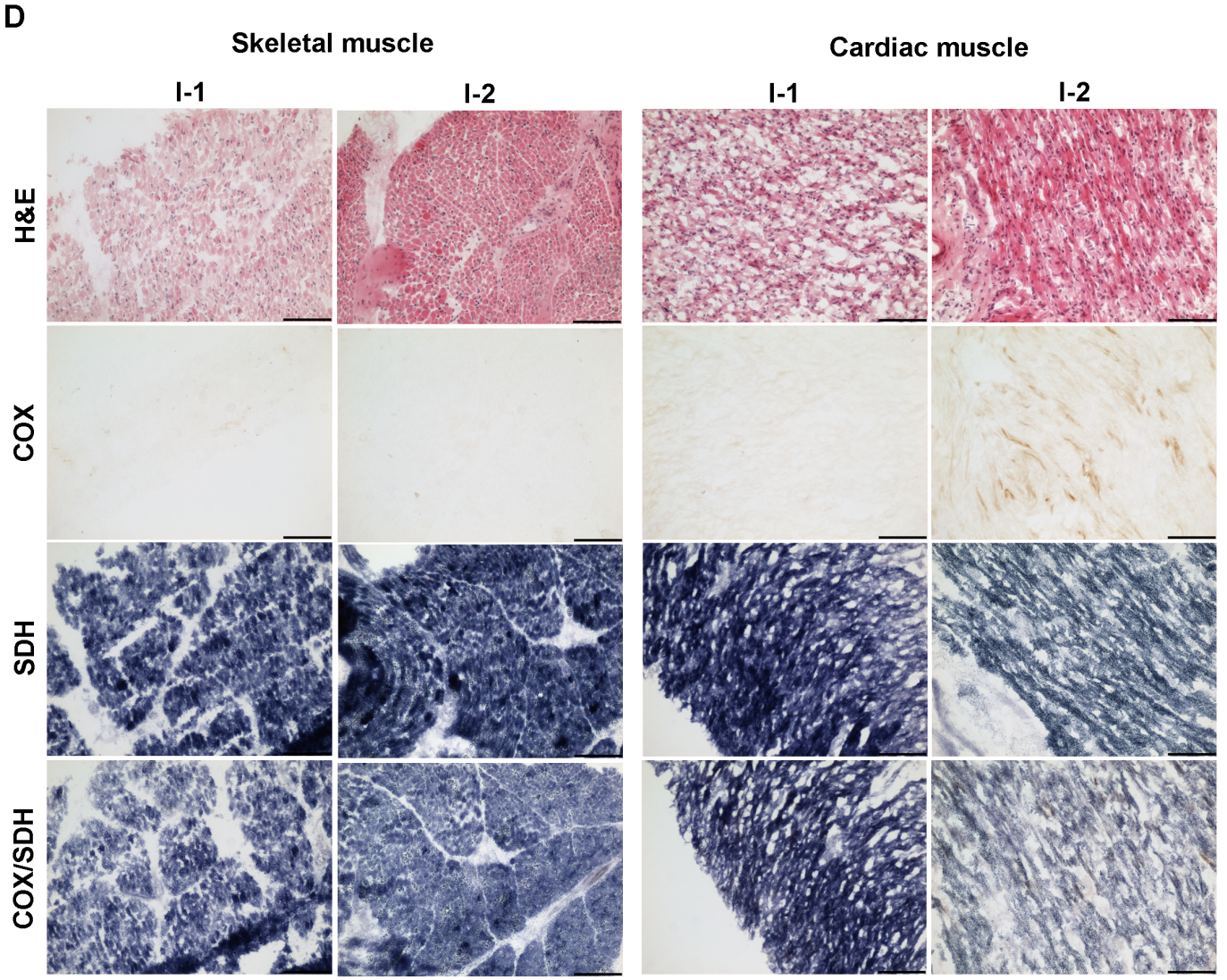

fresh-frozen 10-μm-thick cryosections. Standard methods included hematoxylin and eosin (H&E) stain, modified Gomori trichrome stain, and sequential cytochrome *c* oxidase/succinate dehydrogenase (COX/SDH) histochemistry to assess both complex IV (COX) and complex II (SDH) activities (13). Activities of individual respiratory chain complexes (I–IV) and citrate synthase were measured spectrophotometrically, as previously described (14).

Molecular Genetic Investigations

Genomic DNA was extracted from patient muscle biopsy according to standard protocols. Primer 3 was used to design primers specific to each coding exon of *RARS2* (Figure, Supplemental Digital Content 1, http://links.lww.com/NEN/A746). Patient genomic DNA was polymerase chain reaction (PCR) amplified and Sanger sequenced using BigDye v3.1 chemistry (Applied Biosystems, Cheshire, UK) and capillary electrophoresis performed on an ABI3130xl platform (Applied Biosystems) (15). Patient sequencing chromatograms were compared with the Genbank reference sequence (NM_020320.3) and all variants were annotated using dbSNP build 138. Allele frequency of all gene variants was determined using ESP6500 and 10k genome project data. Parental DNA samples were referred to confirm a recessive inheritance of detected variants.

Complimentary DNA (cDNA) was derived from whole RNA extracted from patient fibroblasts cultured in standard Dulbecco modified eagle medium. Preservation of abnormal mRNA transcripts was accomplished by culturing confluent patient fibroblasts overnight in emetine-containing media at a final concentration of 100 μg/mL before harvesting (16). Reverse transcription of 2 μg RNA was performed using GoScript reverse transcription system and a poly dT primer (Promega, Hampshire, UK). PCR amplification of 2 overlapping cDNA fragments and electrophoresis of PCR amplified products through a 2% agarose gel facilitated identification of normal and abnormal length cDNA fragments.

Gel excision of cDNA fragments was performed using the Agarose Gel DNA Extraction Kit (Roche, Welwyn, Garden City, UK), according to the manufacturer's protocol and recovered amplicons were subject to DNA sequencing. In silico splicing prediction tools NNSPLICE, Human Splicing Finder, and MaxEnt were used to investigate the likely impact of a putative splicing variant in intron 8 identified by cDNA studies.

Neuropathology

Postmortem intervals for Patients I-1 and I-2 were 5 days and 1 day, respectively. After removal of the CNS, frontal and occipital brain samples from Patient I-2 were snap-frozen and kept at −80°C for long-term storage. Peripheral sciatic nerve tissues were also sampled and processed for electron microscopy. For both Patient I-1 and I-2, the remaining CNS was fixed in formalin for 7 and 11 days, respectively, and paraffin embedded before undergoing routine neuropathologic examination (14). To document the severity of the pathologic changes in patient tissues, CNS tissues from 2 disease controls were obtained from the Newcastle Brain Tissue Resource (Table, Supplemental Digital Content 2, http://links.lww.com/NEN/A747). Histology and immunohistochemistry were performed as previously described (14).

Mitochondrial Respiratory Chain Enzyme Histochemistry and Immunohistochemistry

Sequential COX/SDH histochemistry was undertaken on 10-μm-thick frozen sections of frontal and occipital cortex from Patient I-2, as previously described (17). Distribution and expression of key subunits of the mitochondrial respiratory chain complexes (complexes I–IV) and porin (a marker of mitochondrial number) were analyzed using immunohistochemistry performed on 5-μm formalin-fixed, paraffin-embedded frontal, parietal, temporal, and occipital cortices, basal ganglia, pons, and cerebellum, as previously described (14). To allow a direct comparison, patient and control tissues were included in all experiments.

RESULTS

Cranial MRI

Cranial MRI on Day 8 of Patient I-2 showed markedly decreased cerebellar diameter at 33 mm, reduced vermian height at 10.9 mm (Fig. 1A), and slightly decreased anteroposterior pontine diameter at 10 mm but with normal shape. No cerebellar cysts were identified. Cerebrum showed punctate foci in lobar white matter (Fig. 1B); corpus callosum and splenium were within normal limits; there were simple gyri with a possible area of polymicrogyria within 1 Sylvian fissure. Lateral ventricles were prominent. There was no midline fusion of either deep grey matter or cortical ribbon (Fig. 1C).

General Autopsy

Patient I-1

The head circumference was 32.5 cm (50th–75th centile). External gross examination showed no facial or other dysmorphism. Internal gross findings consisted of bilateral pleural effusions, hypoplastic lungs; the heart was normal. Microscopically, liver and kidney were normal.

Patient I-2

Head circumference was 32.0 cm (50th–75th centile). External gross examination revealed generalized subcutaneous edema, small midface, wide lower face, and depressed nasal bridge; limbs, hands, and feet were normal. There were pericardial, pleural, peritoneal effusions. Lungs were hypoplastic. The heart showed prominent right ventricular trabeculation with

FIGURE 1. Cranial MRI performed on Patient I-2 at age 8 days and effect of *RARS2* mutation on COX activity in postmortem skeletal muscle and heart sections. **(A)** Sagittal T1-weighted image demonstrating hypoplastic cerebellar vermis. **(B)** Transverse T1-weighted images illustrating punctate white matter signal changes (white arrows). **(C)** Coronal T1-weighted image illustrates no midline fusion of the deep grey matter or cortical ribbon. **(D)** COX/SDH histochemistry of patient tissues reveals a generalized loss of COX activity in both skeletal muscle and cardiac tissues. Scale bar = 100 μm.

TABLE. Assessment of Respiratory Chain Complex Activities in Postmortem Skeletal and Cardiac Muscle Homogenates From Patient I-2

	Complex I/CS	Complex II/CS	Complex III/CS	Complex IV/CS
Patient I-2 (muscle)	0.019	0.105	0.155	0.051
Controls (n = 25)	0.104 ± 0.036	0.145 ± 0.047	0.554 ± 0.345	1.124 ± 0.511
Patient I-2 (cardiac)	0.008	0.072	0.167	0.015
Controls (n = 25)	0.125 ± 0.048	0.152 ± 0.050	1.112 ± 0.386	1.258 ± 0.367

Enzyme activities are expressed as nmol NADH oxidized min^{-1}.unit citrate synthase $(CS)^{-1}$ for complex I, nmol DCPIP reduced min^{-1}.unit citrate $synthase^{-1}$ for complex II (succinate:ubiquinone-1 reductase) and the apparent first-order rate constant.sec^{-1}.unit citrate $synthase^{-1}$ for complexes III and IV ($\times 10^3$). Control values are shown as mean ± SD. DCPIP, 2,6-dichlorophenol-indophenol.

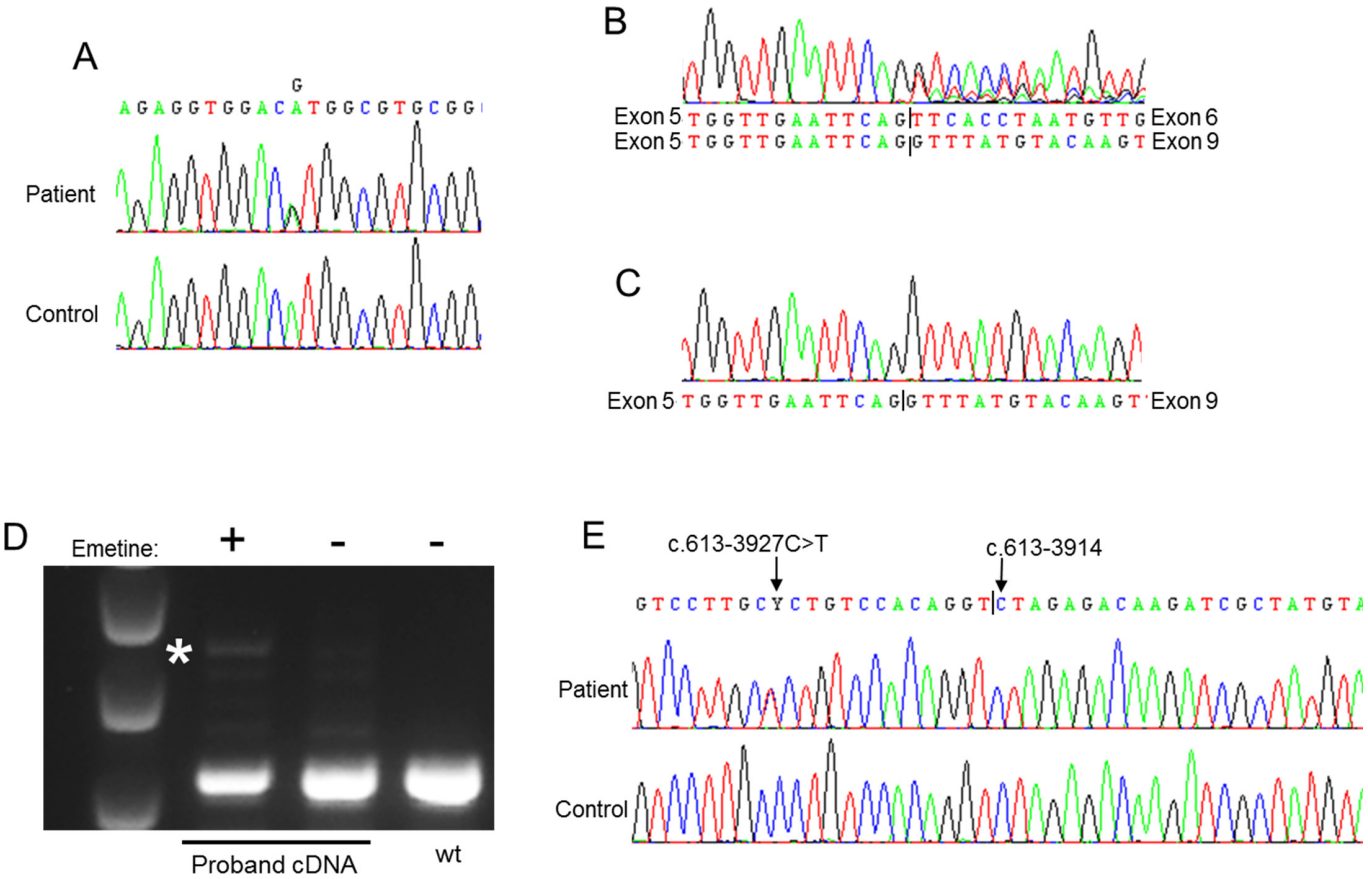

FIGURE 2. Molecular characterization of novel *RARS2* mutations. **(A)** Sequencing of the *RARS2* coding region identified a novel heterozygous c.1A>G *RARS2* variant predicted to abolish the initiating methionine (p.Met1?). **(B)** PCR and electrophoretic analysis of *RARS2* cDNA derived from the proband's fibroblasts revealed 2 populations, a wild-type amplicon plus an amplicon demonstrating skipping of exons 6–9. **(C)** Sequencing of a gel-purified cDNA amplicon clearly shows skipping of exons 6–9 in *RARS2* patient cDNA. **(D)** cDNA analysis of fibroblasts cultured in emetine-containing media reveal a novel transcript (asterisk). Sanger sequencing of this band following agarose gel excision revealed retention of 112 bp of intronic sequence (Figure, Supplemental Digital Content 1, http://links.lww.com/NEN/A746). **(E)** Sequencing of surrounding genomic DNA revealed a novel c.613-3927C>T substitution upstream of the retained intronic sequence, which create a cryptic splicing acceptor at c.613-3916_613-3915; together with a cryptic splicing donor site at c.613-3793_613-3792, this causes the retention of 112 bp of intron 8 (Figure, Supplemental Digital Content 1, http://links.lww.com/NEN/A746).

a thickened (0.9 cm) free ventricular wall. The left ventricle showed less trabeculation, but there was slight thickening of the free wall (1.2 cm); the myocardium was pale. The liver showed centrilobular congestion with focal cholestasis, microsteatosis, and lipid vacuolation of some hepatocytes. Renal tubules featured occasional Oil Red O–positive lipid vacuoles.

Muscle and Cardiac Morphology, Histochemistry, and Biochemistry

Patient I-1

Cardiac muscle featured instances of myocyte central clearing and abundant eosinophilic cytoplasmic puncta interpreted as mitochondria, some abnormally large, overall considered consistent with a mitochondrial cardiomyopathy. Oil Red O stain did not show accumulation of fine-droplet lipid in any myofiber.

Patient I-2

Microscopically, the heart showed myocyte hypertrophy without disarray. Some myocytes were swollen with perinuclear clearing and loss of cross-striation; contained numerous eosinophilic dots interpreted as mitochondria, some being abnormally large; and had an excess of fine droplets of Oil Red O–positive lipid. There was no inflammation, necrosis, or endocardial fibroelastosis.

COX/SDH histochemistry revealed a near global loss of COX activity despite sparing of SDH activity in both skeletal and cardiac muscle tissues from both patients (Fig. 1D). Although the postmortem interval was longer in Patient I-1 (5 days), it is our experience that samples retain COX and SDH activity after considerable postmortem delay and it is usually SDH activity that is most labile. Spectrophotometric assay of mitochondrial respiratory chain complexes showed a marked reduction in complex I, III, and IV activities in Patient I-2's skeletal and cardiac muscle compared with controls with a general sparing of complex II activity, indicating a generalized defect of mitochondrial translation (Table).

Molecular Genetics

The combination of radiologic cerebellar atrophy and multiple mitochondrial respiratory chain defects strongly suggest the diagnosis of PCH6 (OMIM 611523) due to recessive mutations in the *RARS2* gene (5). In confirmation, sequencing the entire coding region and intron-exon boundaries of the *RARS2* gene was performed for Patient I-2, revealing a single heterozygous c.1A>G variant that is predicted to abolish the initiator methionine, thereby resulting in a null allele (Fig. 2A). No further known or potentially pathogenic *RARS2* variants were identified in the coding region. cDNA investigations using fibroblast-derived RNA from Patient I-2 provided evidence of aberrant mRNA splicing with the presence of 2 differentially sized *RARS2* cDNA molecules, the wild-type transcript harboring the c.1A>G variant and a second transcript apparently lacking exons 6, 7, and 8 (Figs. 2B, C). Repeating the cDNA investigations using fibroblasts cultured in emetine, an inhibitor of mitochondrial translation, revealed a number of additional transcripts. One retained 123 bp of intronic sequence from intron 8, c.613-3916_613-3793 (Fig. 2D). Analysis of the surrounding genomic sequence revealed a novel c.613-3927C>T variant upstream of the retained sequence (Fig. 2E; Figure, Supplemental Digital Content 1, http://links.lww.com/NEN/A746), supporting creation of a cryptic splice acceptor. *In silico* investigations predict a very high score for the c.613-3916 cryptic splice acceptor site. The aberrantly spliced mRNA transcript that lacks exons 6–8 results in a frame-shift mutation.

Analysis of familial DNA samples confirmed that both sisters harbored the paternal c.1A>G, p.? and maternal c.613-3927C>T *RARS2* variants, thereby confirming recessive inheritance. Prenatal testing of a chorionic villus sample for these variants in a third pregnancy revealed neither *RARS2* variant and a healthy child was born.

Neuropathology

Patient I-1

The fixed brain was micrencephalic weighing 257 g (reference range, 366 ± 50 g, n = 11 for 36–37 weeks gestation [18]). The combined cerebellum and brainstem weight of 11.5 g was similarly low for the age (reference range, 21.4 g ± 3.36 g). Externally, the gross appearance of forebrain and hindbrain was normal, and the cerebellar vermis and hemispheres were normally formed without any evidence of atrophy. Coronal sectioning of the hemispheres showed cortical pallor, consistent with ischemia-hypoxia, with lobar white matter discoloration without cystic degeneration or mineralization. The corpus callosum, fornix, septum pellucidum, and internal capsule were normal. The deep grey matter was unremarkable and without mineralization. The hippocampi were normal with mild compression in the lateral ventricles. The third ventricle was normal and there was no fusion across the midline. The midbrain aqueduct was compressed in the vertical plane, suggestive of mild cerebral swelling. Tectum and peduncles were normal. Cerebellum was sectioned horizontally and lacked distinct dentate nuclei. Medulla and pons were grossly normal.

Microscopically, the cerebellar cortex revealed focal depletion of neurons from the external granular cell layer, an abnormally thin molecular layer, and sparsely populated internal granular cell layer. Purkinje cell numbers were markedly reduced, with the remainder exhibiting a shrunken perikarya and eosinophilia (Fig. 3Bi). Calbindin-staining demonstrated the perikaryal change and added severe stunting of apical dendrites, with an absence of ''cactus bodies'' (dystrophic dendritic structures) (Fig. 3Biv). The dentate nucleus ribbon, best identified by synaptophysin immunoreactivity (Fig. 3Cii), had a normal undulating configuration but was abnormally thin and was very sparsely populated by neurons in H&E stain (Fig. 3Ci). In the medulla, synaptophysin immunostaining likewise demonstrated a normally formed neuropil ribbon for the inferior olivary nuclei, whereas H&E stain demonstrated its constituent neurons (Figs. 3Di, ii). Pyramidal and other long tracts appeared normal. The basal pontine nuclei contained normal neuron complement, although rare karyorrhectic bodies were identified (Fig. 4Bi). Basal pontine transverse fibers could not be demonstrated using antiphosphorylated neurofilament immunohistochemistry (Fig. 4Ci) contrasting with the positive immunoreactivity in the medial longitudinal fasciculus (Fig. 4Cii) and medial lemniscus (Fig. 4Ciii). The midbrain had a distinct red nucleus, but decussation of superior cerebellar peduncle could not be demonstrated. The cerebral aqueduct, cerebral peduncles,

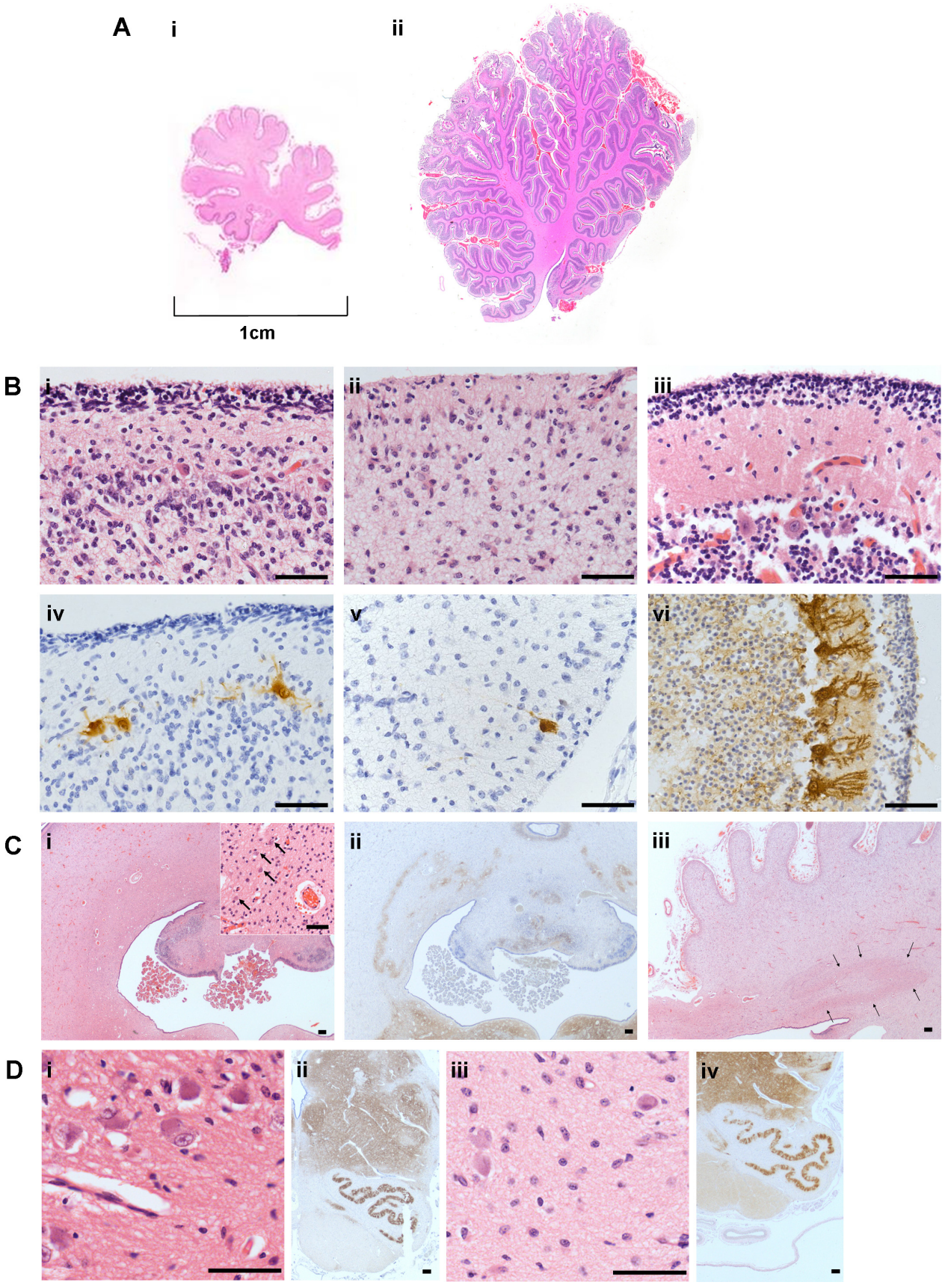

and colliculi were normal. Although the hippocampi were normally formed, there was minor subicular neuronal karyorrhexis, microgliosis, and astrocytosis. Putamen, caudate, globus pallidus, and thalamus had normal neuronal complement, cytology, and neuropil consistency and did not show any mineralization. By immunohistochemistry, only the globus pallidus and lateral nuclei of the thalamus showed diffuse microgliosis; there was no astrocytosis. The optic tract and posterior limb of internal capsule appeared normal. The cerebral white matter was congested but lacked periventricular leukomalacia or other acquired abnormalities and the corpus callosum was normal. The neocortex demonstrated normal neuronal complement and cytology and no mineralization was observed.

Patient I-2

The fixed brain weighed 230 g, whereas the combined brainstem and cerebellum weight was disproportionately low at 10.4 g (4.5% of total fixed brain weight). Externally, cerebral leptomeninges loosely covered a normal arrangement of gyri where there was no sulcal widening. The medulla and cerebellum were much smaller relative to the remainder of the brain. Coronal sections of cerebrum showed neither sulcal widening nor malformation; however, macroscopically, there was dark discoloration of the central white matter with superimposed pale streaks within the occipital region (Fig. 4Di). The corpus callosum was of normal thickness, the anterior commissure and fornix were normal, and the septum pellucidum was caved anteriorly but otherwise normal. The deep grey matter showed no midline fusion. The hippocampi appeared normally formed and largely filled the temporal horns; the lateral and third ventricles were not dilated. The midbrain showed a normal aqueduct, peduncles, and colliculi. Pons had grossly normal tegmentum and basis pontis, whereas the medulla was tiny. Cerebellar vermis and hemisphere showed fewer folial subdivisions than normal (Figs. 3Ai, ii). A 5-cm sample of lower spinal cord displayed no convincing abnormalities.

Microscopic findings were generally similar to or supplemented those in the sibling. Sagittal sections through the cerebellar vermis clearly demonstrated a normal arrangement of principal lobules but much reduced folial branching (Fig. 3Ai). The marked reduction in thickness of individual cortical laminae, lack of Purkinje cells (Fig. 3Biii) and their cytologic changes (Fig. 3Bv), and reduced internal granule-cell packing-density were as in Patient I-1. The dentate nucleus and the internal olivary nuclei were both discernible and normally formed (Figs. 3Ciii and Diii, iv). The basis pontis of Patient I-2, however, contrasted strikingly with her sister's by displaying marked neuron loss (Fig. 4Bii) associated with astrogliosis (Fig. 4Biii), and microgliosis (Fig. 4Biv). Deep cerebral white matter showed mineralizing macrophage-rich foci of periventricular leukomalacia (Fig. 4Dii), corresponding to the macroscopic streaky pallor. The putamen, caudate, and globus pallidus exhibited sparse eosinophilic neurons consistent with ischemia-hypoxia, capillary prominence, and endothelial cell hypertrophy without excessive micromineralization. Immunohistochemistry for glial fibrillary acidic protein showed astrocytosis in the globus pallidus alone, whereas anti-CD68 showed moderate and minor microgliosis in globus pallidus and caudate-putamen, respectively. The hypothalamus showed normal nuclear groups and mammillary bodies, dorsolateral regions showed moderate diffuse microgliosis, and there was no astrocytosis. In contrast to Patient I-1, the internal capsule and optic tract showed moderate microgliosis.

Sciatic nerve (available for Patient I-2 only) showed rare small CD68-positive macrophages and similarly immunoreactive sparse spindly cells within the endoneurium by light microscopy. Phosphorylated neurofilament antibody showed axons of all sizes (Figs. 5A, B). There were no cellular infiltrates. Electron microscopy, although hampered by postmortem artefact, demonstrated considerably fewer myelinated fibers than expected for the age (Figs. 5C, D). Some myelinated fibers had an inappropriately thin sheath for axon diameter. In some others, the axon was absent, leaving only a collapsed myelin sheath. A few unmyelinated axons were large enough to be the result of demyelination, whereas the perineurium appeared mature, which does not suggest delayed maturation.

Mitochondrial Pathology in CNS Tissues

Mitochondrial densities, as judged by porin and nuclear-encoded SDHA immunoreactivity, were high in neurons throughout all CNS tissues analyzed. Immunohistochemical analysis of mitochondrial respiratory chain protein expression showed evidence of a specific and total loss of subunits comprising complex I, as judged by a lack of immunoreactivity for subunits NDUFB8 and NDUFS3, throughout all CNS tissues investigated in both Patients I-1 and I-2. This was prominent in the cerebellum where cell loss was severe (Fig. 6), the pontine nucleus (Fig. 7), and in other regions where neuronal population density was intact, including the occipital cortex (Fig. 8) and other brain regions, including frontal cortex and basal ganglia (Figure, Supplemental Digital Content 3, http://links.lww.com/NEN/A748). Analysis of the other mitochondrial respiratory chain complexes revealed comparable immunoreactivity of complexes II and III to that observed in control tissues; however, the mitochondrially encoded COX1 was absent despite high immunoreactivity for COX4 of this complex. This loss of protein expression is selective for complexes I and COX1 throughout the brain and suggestive of respiratory chain deficiency due to decrease or absence

FIGURE 3. Histopathologic findings in the cerebellar tissues from Patient I-1 and I-2. **(A)** Macroscopically, the delayed development of the cerebellum is prominent in Patient I-2 (i) compared with an age-matched control (ii, H&E). **(B)** At a higher magnification, there is a marked reduction in Purkinje cells by H&E in both patients (I-1 = i, I-2 = ii) relative to an age-matched control (iii). Where Purkinje cells were present in Patient I-1 (iv) and Patient I-2 (v), they exhibited stunted apical dendrites compared with those in an age-matched control (vi). Calbindin immunohistochemistry. **(C)** The dentate nucleus was detected in both cases although the neuronal population density was reduced in Patient I-1 (i) and I-2 (iii), and the neuropil ribbon was thin (I-1, ii, synaptophysin). **(D)** The inferior olivary nuclei were present in both cases with intact neuronal population density shown with H&E in Patient I-1 (i) and Patient I-2 (iii). Neuropil ribbons are demonstrated in Patient I-1 (ii, synaptophysin) and I-2 (iv, synaptophysin). Scale bar = 100 μm.

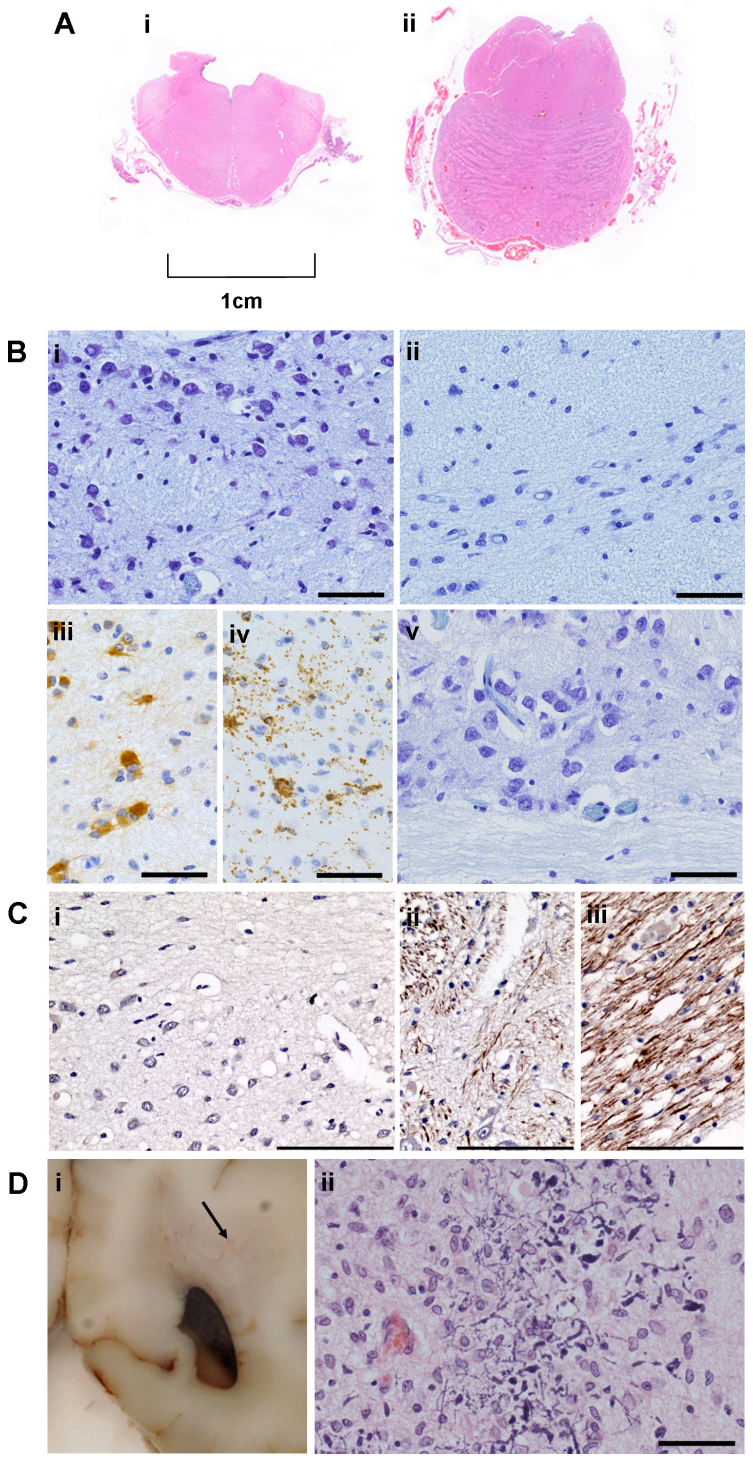

FIGURE 4. Histopathologic findings in the pons and occipital lobe tissues from Patient I-1 and I-2. **(A)** Macroscopic assessment of H&E-stained pons from Patient I-2 (i) revealed severe atrophy compared to an age-matched control (ii). **(B)** In a pontine nucleus in Patient I-1, there is relatively intact neuronal cell density (Luxol Fast Blue with Cresyl Fast Violet [LFB/CFV]) (i), whereas there was marked neuronal cell loss in Patient I-2 (ii, LFB/CFV) accompanied by astrogliosis (iii, glial fibrillary acidic protein immunohistochemistry [IHC]) and microgliosis (iv, CD-68 IHC), which was in contrast to normal neuronal density in an age-matched control (v, LFB/CFV). **(C)** In addition, there is a profound loss of phosphorylated neurofilaments in axons corresponding to the pontocerebellar fibers in Patient I-1 (i, SMI-31R IHC) in contrast to intact expression in medial longitudinal fasciculus (ii) and medial lemniscus (iii). **(D)** Deep white matter abnormalities were observed in the occipital lobe (i), consistent with the hyperintensity seen on neuroimaging; microscopically, this corresponded to the presence of mineralized axons (ii, H&E). Scale bar = 100 μm.

of expression of these components despite abundant mitochondria in these regions.

DISCUSSION

We present only the second autopsy series of neonatal pontocerebellar hypoplasia type 6 (PCH6) in 2 siblings born to nonconsanguineous parents. In the neonatal period, the siblings were hypotonic, lacked spontaneous respiratory effort, and deteriorated rapidly, leading to death on Day 1 and Day 14, respectively. Biochemical analysis of skeletal and cardiac muscle confirmed extensive respiratory chain deficiency involving complexes I, III, and IV, and enzyme histochemistry showed a complete loss of COX activity. Mitochondrial respiratory chain complex-specific immunohistochemistry confirmed a lack of immunoreactivity for complexes I and IV despite a high density of mitochondria throughout the CNS. This supports a generalized loss of respiratory chain activity due to a translation defect and is in agreement with previous findings with variable respiratory chain defects in muscle from patients with *RARS2* mutations (5, 10). Molecular genetic investigations identified a paternally inherited single heterozygous c.1A>G mutation that is predicted to abolish translation initiation. Despite the identification of just 1 heterozygous *RARS2* variant, the certain pathogenicity meant that it was highly likely that PCH6 was the clinical diagnosis in tandem with a second, latent *RARS2* variant. This initiated cDNA studies that led to the identification of a cDNA transcript lacking exons 6–8 due to a maternally

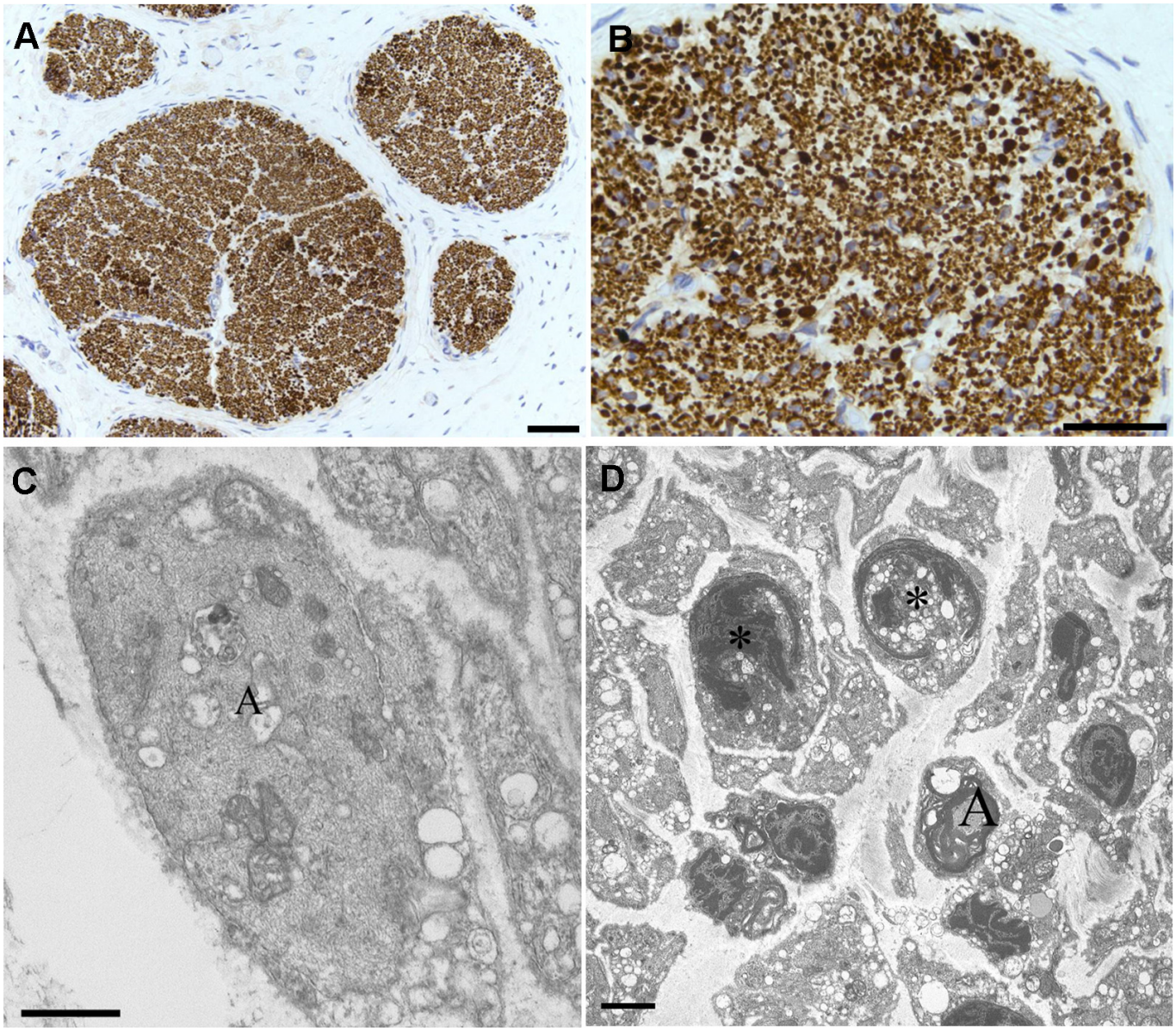

FIGURE 5. Sciatic nerve pathology in Patient I-2. **(A, B)** IHC revealed an irregular distribution and reduced number of large axons in the sciatic nerve (neurofilament IHC). **(C, D)** Electron microscopy revealed loss of myelin surrounding axons [A] and the presence of degenerating fibers (*), which are observed alongside intact axons. Scale bars: **A, B**, 100 μm; **C**, 1 μm; **D**, 2 μm.

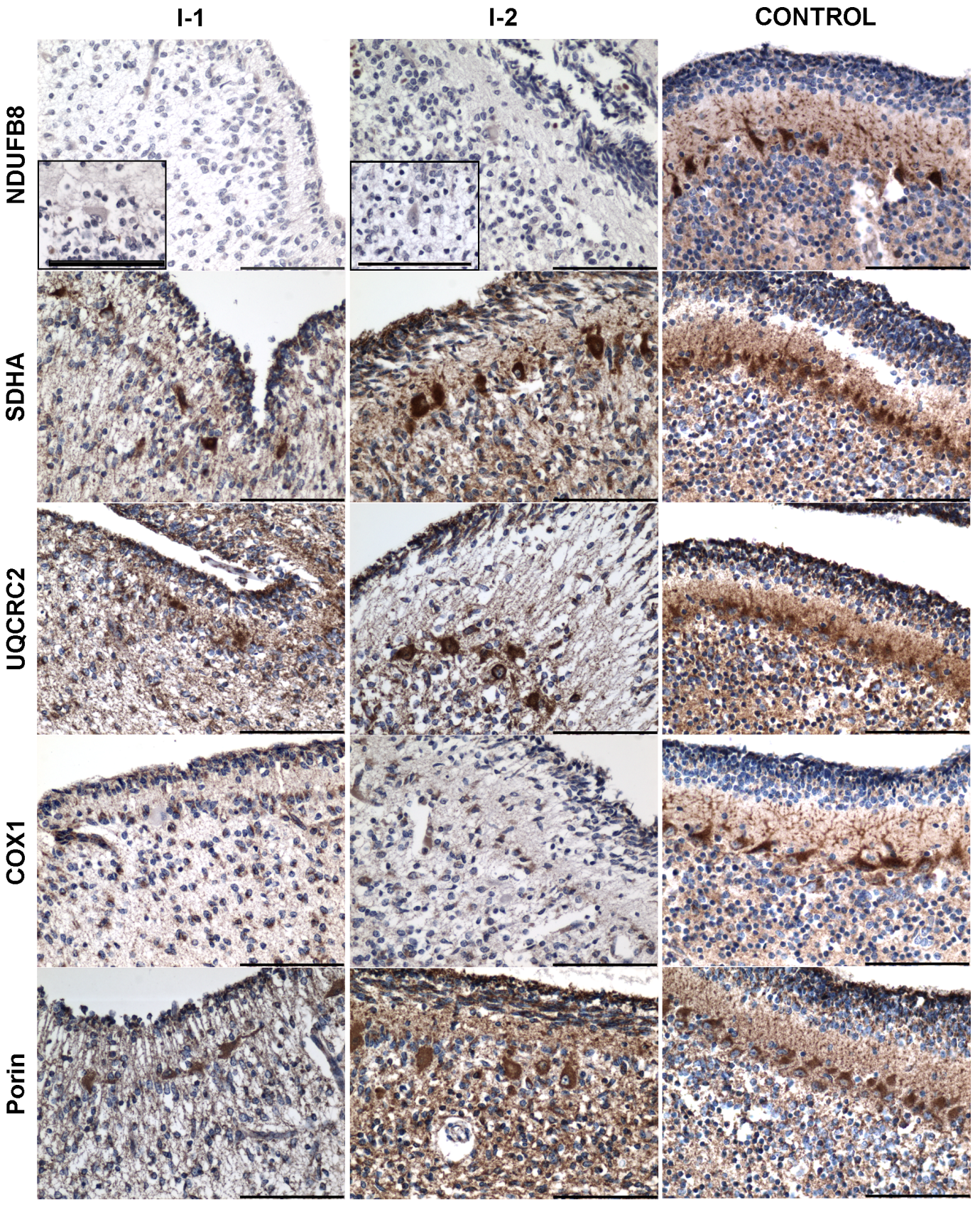

inherited novel, deep-intronic variant, c.613-3927C>T, which activates a cryptic splice site. In addition to reporting 2 novel *RARS2* mutations, this study expands upon the clinical phenotypes and neuropathology associated with *RARS2* mutations in this rare autosomal recessive mitochondrial disease.

The canonical features of PCH6 detected in Patient I-2 included early-onset encephalopathy, raised lactate levels in blood and CSF, pontocerebellar hypoplasia (observed on MRI and confirmed by neuropathologic examination), and combined defects in oxidative phosphorylation (5, 7, 9, 10). In addition, we report features not previously associated with PCH6 including fetal echocardiograph findings consistent with a hypertrophic cardiomyopathy phenotype and hydrops fetalis. Cardiomyopathy was detected at 20 weeks gestation following concerns regarding fetal bradycardia and was ascribed to biventricular hypertrophy. Despite being a new finding in association with *RARS2* mutations, cardiomyopathy is a common clinical feature in other mitochondrial disease presentations in which neonatal presentation of the hypertrophic type (HCM) is associated with a high mortality (19). The high rate of mortality might reflect the metabolic shift from prenatal anaerobic glycolysis to postnatal metabolism that is driven by fatty acid oxidation, ketone catabolism, and oxidative phosphorylation (20). Primary mutations affecting mitochondrial DNA and mutations in the nuclear-encoded alanyl-tRNA synthetase (*AARS2*), *MTO1*, and *GTBP3* genes have also been implicated in severe infantile, prenatal-onset cardiomyopathy presentations with combined respiratory chain deficiencies (21–23). In addition to HCM, pulmonary hypoplasia was also reported in the patients described by Gotz et al and was thought to be secondary to the cardiac hypertrophy (23).

In view of the neuroradiologic imaging supporting the clinical diagnosis of PCH6, sequence analysis of the *RARS2* gene was undertaken. Sixteen PCH6 patients with recessive *RARS2* mutations have been reported to date, with missense variants being the major class (24). There is a paucity of truncating mutations, highlighting the importance of the full-length, functional transcript although splicing variants have accounted for 1 allele in 10 patients. No patient reported to date has presented with 2 null *RARS2* alleles, and this is reflected also in this family. The c.1A>G variant is predicted to entirely abolish the translation of the corresponding allele, whereas we hypothesize that the allele harboring the deep intronic splicing variant is predicted to confer some (albeit minimal) residual activity due to some normal transcript remaining. This would explain the limited compatibility with life that was observed in the clinically affected children of this family.

As a mutational mechanism, deep intronic variants are likely to be under-represented in the literature, possibly as a consequence of strategies employed in current genetic testing. First, genomic DNA is often the source for diagnostic sequencing investigations; therefore, splicing variants may remain undiagnosed unless they affect the consensus splicing donor or acceptor sites at +/−2 bp of the exon boundary; variants situated beyond +/− 10 bp of the exon/intron boundaries are often regarded as of ''uncertain significance.'' Exome-based, next-generation sequencing strategies share the same bias, although cDNA-based next-generation sequencing strategies and whole genome sequencing will hopefully elucidate the prevalence of both splicing variants and large-scale gene rearrangements. The deep intronic *RARS2* variant was only apparent following emetine-induced nonsense mediated decay arrest; the abnormal transcript was subject to nonsense mediated decay in normal culture conditions, leaving only a transcript lacking exons 6–8 in the mRNA corresponding to the maternal allele. This variant, although not subject to nonsense mediated decay, is likely to give rise to a nonfunctional, truncated protein. To our knowledge, only 1 deep intronic mutation has been reported previously in association with any mitochondrial disease presentation—a dominant *OPA1* mutation that causes progressive optic atrophy in adulthood (25). In addition to describing the first deep intronic recessive mutation in a fatal pediatric mitochondrial disease presentation, this study highlights the utility of cDNA investigations, particularly in patients with only 1 candidate mutation in a recessively inherited disease.

There is only 1 illustrated report of PCH6 neuropathology describing 2 cases (11), and 1 very brief description as part of a broader survey of pontocerebellar hypoplasia (7). Therefore, our findings double the number of neuropathologic descriptions of this condition and provide the first record of peripheral nerve pathology.

Our findings are similar to those of Joseph et al (11) in a number of respects but also reveal some significant differences. We found that the brains of our patients were also micrencephalic and the cerebellar vermis displayed much-simplified foliation, corresponding, at a rough estimate (26), to that of a 114-mm crown-rump (~18 week gestation) fetus and indicating an element of developmental delay, or arrest, that began in utero, in agreement with previous findings (11). The pons was abnormally small and basal pontine nucleus neurons were severely decreased in number in Patient I-2 but were within normal limits in Patient I-1. The small size of the pons might be attributed to delayed development, whereas neuronal cell loss might reflect regressive degeneration because of the presence of astrogliosis and microgliosis. Evidence in support of regressive degeneration is provided by the sibling who died only 1 hour after birth and who demonstrated intact neuronal density in the pontine nucleus. This was also verified by Joseph et al, where very few neurons were noted in this structure in both twins. This suggests that *RARS2* mutations adversely affect the pons and cerebellum and that the neurons within these structures are particularly vulnerable to degeneration. In fact, vulnerability of the developed cerebellum to perturbed mitochondrial function is particularly common (27–29). In these cases, however, it is likely to be a direct consequence of a

FIGURE 6. Mitochondrial respiratory chain deficiency in the cerebellum of Patients I-1 and I-2. Immunohistochemical staining of components of the mitochondrial respiratory chain revealed severe, combined respiratory chain deficiencies in remaining cells involving complex I (NDUFB8) and the mitochondrially encoded complex IV subunit I (COX1), despite preservation of complex II (SDHA) and complex III core 2 (UQCRC2) expression and the mitochondrial mass marker porin in serial sections. Scale bar = 100 μm.

mismatch between mitochondrial protein synthesis and the accelerated growth phase of the cerebellum during late gestation, rendering the cerebellum particularly susceptible (30).

We also provide further evidence corroborating deep white matter pathology in the occipital poles both radiologically and histopathologically that is comparable with the findings of Joseph

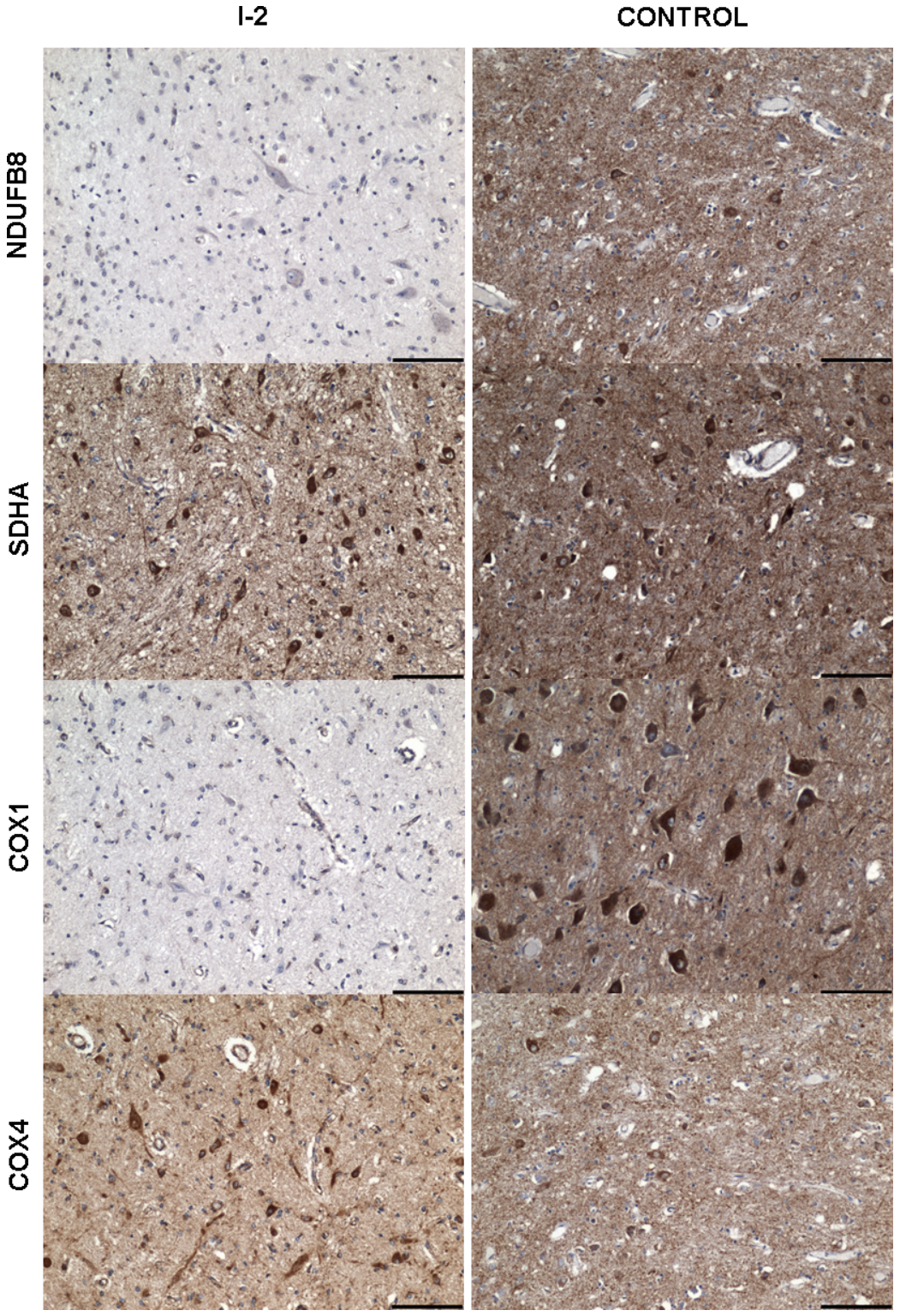

FIGURE 7. Mitochondrial respiratory chain deficiencies in the pontine nucleus. The mitochondrial respiratory chain proteins investigated showed high immunoreactivity in an age-matched control (right panels). Patient I-2 shows a profound absence of immunoreactivity for complexes I (NDUFB8) and IV (COX1), indicating respiratory chain deficiency. Scale bar = 100 μm.

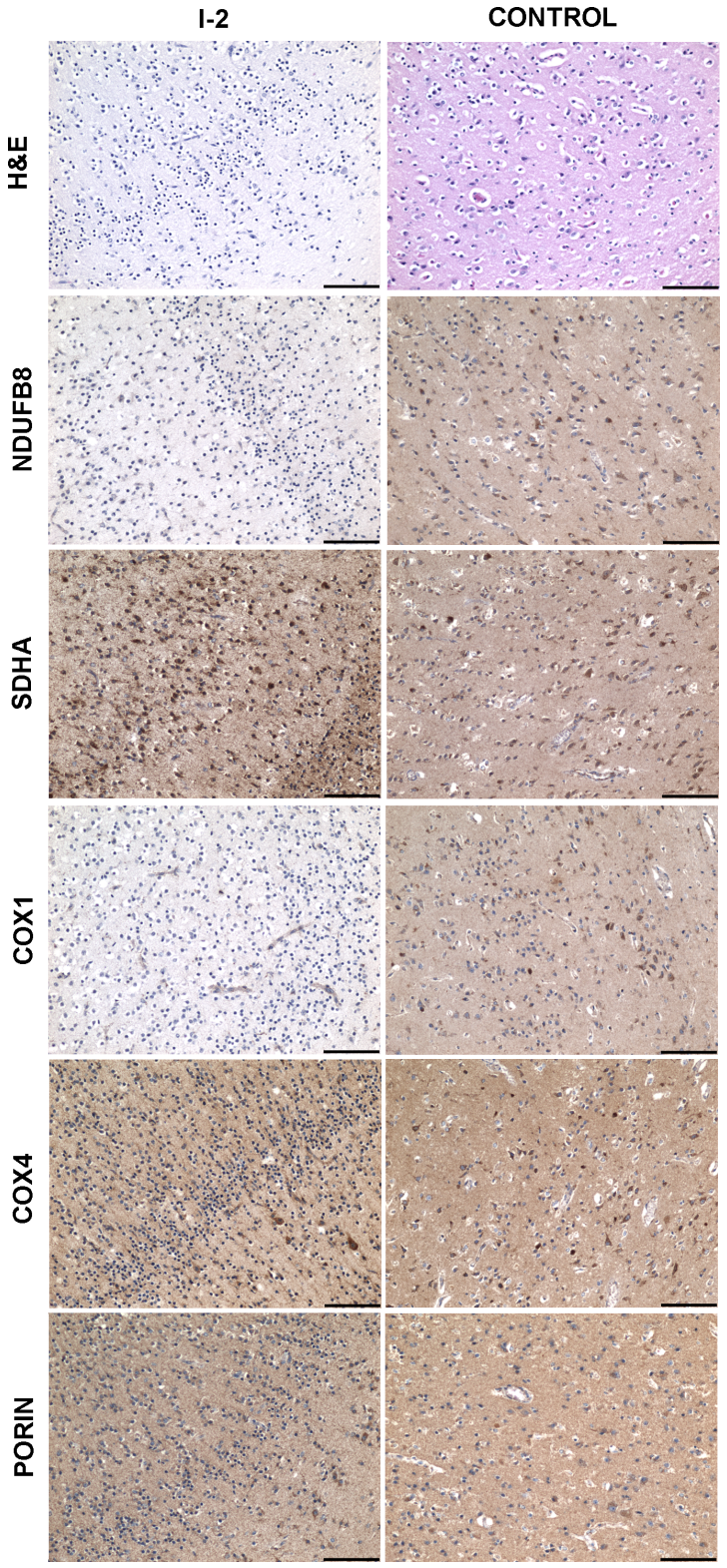

FIGURE 8. Mitochondrial respiratory chain deficiency in the occipital cortex. Neuron population densities were intact in Patient I-2 and control tissues (H&E). Immunohistochemical staining for components of the mitochondrial respiratory chain revealed a marked loss of complex I in Patient I-2 (NDUFB8) vs control (NDUFB8), and mitochondrially encoded subunit of complex IV (COX1) vs control (COX1), indicating complex I and IV deficiencies. Complex II (SDHA) and a nuclear-encoded subunit of complex IV (COX4) expression levels were preserved in conjunction with high mitochondrial density (porin) in both patient and control neurons. Scale bar = 100 μm.

et al, with discoloration, extensive gliosis, and few neurofilaments. Since both of our patients exhibited clinical complications associated with poor ventilation due to respiratory insufficiency, we cannot exclude the effects of hypoxic-ischemic injury contributing to the presence of karyorrhectic neurons in the pons and subiculum, eosinophilic neurons in the basal ganglia, and also periventricular leukomalacia. This was not a striking feature of the patients described by Joseph et al, but it remains an important consideration when evaluating the neuropathology since these are often features that emerge after severe hypoxic-ischemia (31).

We observed additional novel features not previously documented in PCH6 that expand on the neuropathologic features of the disorder. In both siblings, we identified the cerebellar dentate nucleus and inferior olivary nucleus, although we recognize the former demonstrated reduced neuronal cell density and gliosis. We were also able to identify a red nucleus, which was gliotic in Patient I-1. MRI in our cases did not reveal midline fusion of cerebral deep white matter and confirmed a full corpus callosum with well-formed splenium, in contrast to the findings of Joseph et al. Another important novel finding was the evidence of reduced axonal packing density and abnormally thin myelin sheaths in the peripheral nerve, which has not previously been described in PCH6.

Mitochondrial respiratory chain complex-specific immunohistochemistry was investigated in CNS tissues for the first time in both patients. This analysis revealed profound and rather selective complex I and IV deficiency, involving complex I subunits NDUFB8 and NDUFS3 and mitochondrially encoded COX1. This pattern of respiratory chain deficiency was widespread and not just restricted to the brainstem and cerebellum where the greatest pathology was evident.

The present study expands on the disease-causing variants of *RARS2*, provides further evidence of the clinical heterogeneity associated with *RARS2* mutations, and augments the neuropathologic features associated with PCH6. Our data expand on the pathogenesis of PCH6 disease caused by *RARS2* mutations and provide further characterization of the specific temporal and regional degeneration in patients with this rare disorder. Neuronal tissue is exquisitely sensitive to deregulation of protein synthesis, and even more so during the postmigratory phase of neuronal development when the demand for protein synthesis is high. Although we understand that RARS2 encodes for an enzyme that aminoacylates mt-tRNA^{Arg} in mitochondria, we do not fully understand why mutations in this gene cause a specific pattern of neurodegeneration leading to PCH6. We can speculate on the mechanisms based on *TSEN54* and *RARS2* knockdown studies performed in zebrafish in which overlapping phenotypes are observed implying a shared mechanism of degeneration (32). Based on this, we speculate that the demand for mitochondrial arginyl-tRNA synthetase is particularly high during the development of certain tissues, including the pontocerebellar and cardiac tissues. Indeed, the cerebellum undergoes a rapid phase of growth during late gestation, that is, at 28 weeks postconception, which could explain the specific vulnerability of this brain region to impaired *RARS2* function in patients harboring *RARS2* mutations (30).

Establishing a genetic diagnosis for families with mitochondrial respiratory chain dysfunction is crucial in the process of genetic counseling enabling a correct recurrence risk to be provided and reproductive options including prenatal diagnosis or preimplantation genetic diagnosis. Once 2 deleterious *RARS2* gene variants were identified, the parents of the patients in this report opted for analysis of a chorionic villus biopsy in a subsequent pregnancy. Our analysis showed that the fetus harbored neither of the familial *RARS2* mutations and a healthy boy has since been born.

ACKNOWLEDGMENTS

The authors thank Dr E. Hook and Dr A. Whitehead for their help in the general pathological assessment, and biomedical, medical-photographic and secretarial staff at Addenbrooke's Hospital for excellent support.

REFERENCES

1. Skladal D, Halliday J, Thorburn DR. Minimum birth prevalence of mitochondrial respiratory chain disorders in children. Brain 2003;126:1905–12
2. Taylor RW, Pyle A, Griffin H, et al. Use of whole-exome sequencing to determine the genetic basis of multiple mitochondrial respiratory chain complex deficiencies. JAMA 2014;312:68–77
3. Diodato D, Ghezzi D, Tiranti V. The mitochondrial aminoacyl tRNA synthetases: genes and syndromes. Int J Cell Biol 2014;2014:787956
4. Smits P, Smeitink J, van den Heuvel L. Mitochondrial translation and beyond: processes implicated in combined oxidative phosphorylation deficiencies. J Biomed Biotech 2010;2010:737385
5. Edvardson S, Shaag A, Kolesnikova O, et al. Deleterious mutation in the mitochondrial arginyl-transfer RNA synthetase gene is associated with pontocerebellar hypoplasia. American J Hum Gen 2007;81:857–62
6. Rankin J, Brown R, Dobyns WB, et al. Pontocerebellar hypoplasia type 6: A British case with PEHO-like features. AmJ Med Gen Part A 2010;152A:2079–84
7. Namavar Y, Barth PG, Kasher PR, et al. Clinical, neuroradiological and genetic findings in pontocerebellar hypoplasia. Brain 2011;134:143–56
8. Kastrissianakis K, Anand G, Quaghebeur G, et al. Subdural effusions and lack of early pontocerebellar hypoplasia in siblings with RARS2 mutations. Arch Dis Child 2013;98:1004–7
9. Glamuzina E, Brown R, Hogarth K, et al. Further delineation of pontocerebellar hypoplasia type 6 due to mutations in the gene encoding mitochondrial arginyl-tRNA synthetase, RARS2. J Inher Metab Dis 2012;35:459–67
10. Cassandrini D, Cilio MR, Bianchi M, et al. Pontocerebellar hypoplasia type 6 caused by mutations in RARS2: definition of the clinical spectrum and molecular findings in five patients. J Inher Metab Dis 2013;36:43–53
11. Joseph JT, Innes AM, Smith AC, et al. Neuropathologic features of pontocerebellar hypoplasia type 6. J Neuropathol Exp Neurol 2014;73:1009–25
12. Wright D, Kagan KO, Molina FS, et al. A mixture model of nuchal translucency thickness in screening for chromosomal defects. Ultrasound Obstet Gynecol 2008;31:376–83
13. Old SL, Johnson MA. Methods of microphotometric assay of succinate dehydrogenase and cytochrome c oxidase activities for use on human skeletal muscle. Histochem J 1989;21:545–55
14. Lax NZ, Gnanapavan S, Dowson SJ, et al. Early-onset cataracts, spastic paraparesis, and ataxia caused by a novel mitochondrial tRNAGlu (MT-TE) gene mutation causing severe complex I deficiency: a clinical, molecular, and neuropathologic study. J Neuropathol Exp Neurol 2013;72:164–75
15. Untergasser A, Cutcutache I, Koressaar T, et al. Primer3—new capabilities and interfaces. Nucleic Acids Res 2012;40:e115
16. Noensie EN, Dietz HC. A strategy for disease gene identification through nonsense-mediated mRNA decay inhibition. Nature Biotechnol 2001;19:434–9
17. Betts J, Jaros E, Perry RH, et al. Molecular neuropathology of MELAS: level of heteroplasmy in individual neurones and evidence of extensive vascular involvement. Neuropathol Appl Neurobiol 2006;32:359–73

18. Guihard-Costa AM, Larroche JC. Differential growth between the fetal brain and its infratentorial part. Early Hum Devel 1990;23:27–40
19. Schiff M, Ogier de Baulny H, Lombes A. Neonatal cardiomyopathies and metabolic crises due to oxidative phosphorylation defects. Sem Fetal Neonatal Med 2011;16:216–21
20. Lopaschuk GD, Jaswal JS. Energy metabolic phenotype of the cardiomyocyte during development, differentiation, and postnatal maturation. J Cardiovasc Pharm 2010;56:130–40
21. Kopajtich R, Nicholls TJ, Rorbach J, et al. Mutations in GTPBP3 cause a mitochondrial translation defect associated with hypertrophic cardiomyopathy, lactic acidosis, and encephalopathy. Am J Hum Gen 2014;95:708–20
22. Ghezzi D, Baruffini E, Haack TB, et al. Mutations of the mitochondrial-tRNA modifier MTO1 cause hypertrophic cardiomyopathy and lactic acidosis. Am J Hum Gen 2012;90:1079–87
23. Gotz A, Tyynismaa H, Euro L, et al. Exome sequencing identifies mitochondrial alanyl-tRNA synthetase mutations in infantile mitochondrial cardiomyopathy. Am J Hum Gen 2011;88:635–42
24. Grefsheim SF, Whitmore SC, Rapp BA, et al. The informationist: building evidence for an emerging health profession. J Med Libr Assoc 2010;98:147–56
25. Bonifert T, Karle KN, Tonagel F, et al. Pure and syndromic optic atrophy explained by deep intronic OPA1 mutations and an intralocus modifier. Brain 2014;137:2164–77
26. Larsell O, Jansen J, Korneliussen HK, Mugnaini E. *The Comparative Anatomy and Histology of the Cerebellum: The Human Cerebellum, Cerebellar Connections, and Cerebellar Cortex*. Minneapolis, MN. Minnesota University Press, 1972
27. Hakonen AH, Goffart S, Marjavaara S, et al. Infantile-onset spinocerebellar ataxia and mitochondrial recessive ataxia syndrome are associated with neuronal complex I defect and mtDNA depletion. Hum Molec Gen 2008; 17:3822–35
28. Quintana A, Kruse SE, Kapur RP, et al. Complex I deficiency due to loss of Ndufs4 in the brain results in progressive encephalopathy resembling Leigh syndrome. Proc Natl Acad Sci USA 2010;107: 10996–1001
29. Lax NZ, Hepplewhite PD, Reeve AK, et al. Cerebellar ataxia in patients with mitochondrial DNA disease: a molecular clinicopathological study. J Neuropathol Exp Neurol 2012;71:148–61
30. Limperopoulos C, Soul JS, Gauvreau K, et al. Late gestation cerebellar growth is rapid and impeded by premature birth. Pediatrics 2005;115:688–95
31. Lai MC, Yang SN. Perinatal hypoxic-ischemic encephalopathy. J Biomed Biotechnol 2011;2011:609813
32. Kasher PR, Namavar Y, van Tijn P, et al. Impairment of the tRNA-splicing endonuclease subunit 54 (tsen54) gene causes neurological abnormalities and larval death in zebrafish models of pontocerebellar hypoplasia. Hum Molec Gen 2011;20:1574–84

